Three regularization models of the Navier–Stokes equations

Jonathan Pietarila Graham,[1,a)] Darryl D. Holm,[2,3] Pablo D. Mininni,[1,4] and Annick Pouquet[1]
[1]*National Center for Atmospheric Research, P.O. Box 3000, Boulder, Colorado 80307, USA*
[2]*Department of Mathematics, Imperial College London, London SW72AZ, United Kingdom*
[3]*Computer and Computational Science Division, Los Alamos National Laboratory, Los Alamos, New Mexico 87545, USA*
[4]*Departamento de Física, Facultad de Ciencias Exactas y Naturales, Universidad de Buenos Aires, Ciudad Universitaria, 1428 Buenos Aires, Argentina*

(Received 21 August 2007; accepted 16 January 2008; published online 17 March 2008)

We determine how the differences in the treatment of the subfilter-scale physics affect the properties of the flow for three closely related regularizations of Navier–Stokes. The consequences on the applicability of the regularizations as subgrid-scale (SGS) models are also shown by examining their effects on superfilter-scale properties. Numerical solutions of the Clark-α model are compared to two previously employed regularizations, the Lagrangian-averaged Navier–Stokes α-model (LANS-α) and Leray-α, albeit at significantly higher Reynolds number than previous studies, namely, $\mathrm{Re}\approx 3300$, Taylor Reynolds number of $\mathrm{Re}_\lambda \approx 790$, and to a direct numerical simulation (DNS) of the Navier–Stokes equations. We derive the de Kármán–Howarth equation for both the Clark-α and Leray-α models. We confirm one of two possible scalings resulting from this equation for Clark-α as well as its associated k^{-1} energy spectrum. At subfilter scales, Clark-α possesses similar total dissipation and characteristic time to reach a statistical turbulent steady state as Navier–Stokes, but exhibits greater intermittency. As a SGS model, Clark-α reproduces the large-scale energy spectrum and intermittency properties of the DNS. For the Leray-α model, increasing the filter width α decreases the nonlinearity and, hence, the effective Reynolds number is substantially decreased. Therefore, even for the smallest value of α studied Leray-α was inadequate as a SGS model. The LANS-α energy spectrum $\sim k^1$, consistent with its so-called "rigid bodies," precludes a reproduction of the large-scale energy spectrum of the DNS at high Re while achieving a large reduction in numerical resolution. We find, however, that this same feature reduces its intermittency compared to Clark-α (which shares a similar de Kármán–Howarth equation). Clark-α is found to be the best approximation for reproducing the total dissipation rate and the energy spectrum at scales larger than α, whereas high-order intermittency properties for larger values of α are best reproduced by LANS-α. © *2008 American Institute of Physics*. [DOI: 10.1063/1.2880275]

I. INTRODUCTION

Nonlinearities prevail in fluid dynamics when the Reynolds number Re is large.[1] For geophysical flows, the Reynolds number is often larger than 10^8 and for some astrophysical flows values of $\mathrm{Re}\approx 10^{18}$ is not unreasonable. The number of degrees of freedom (dof) in the flow increases as $\mathrm{Re}^{9/4}$ for $\mathrm{Re}\gg 1$ in the Kolmogorov framework[2–4] (hereafter, K41). Such a huge number of dof makes direct numerical simulations (DNS) of turbulence at high Re infeasible on any existing or projected computer for decades to come. Because of this intractability, simulations of turbulence are always carried out in regions of parameter space far from the observed values, either with (a) an unphysical lack of scale separation between the energy-containing, inertial, and dissipative ranges while parametrizing the missing physics, or (b) a study of the processes at much smaller length scales, often with periodic boundaries (unphysical at large scales but used under the hypothesis of homogeneity of turbulent flows). Clearly, modeling of unresolved small scales is necessary.

Given the nonlinear nature of turbulent flows and the ensuing multiscale interactions, the physics of the unresolvable scales may not be separable from the properties (e.g., statistics) of the resolvable large scales. However, two main approaches have been developed over the years to model the effects of the unresolvable small scales in turbulence on the scales resolved in the simulations. The first approach is large eddy simulations[5] (LES). LES is widely used in engineering, in atmospheric sciences, and to a lesser extent in astrophysics. However, in the LES approach, the Reynolds number is not known. Instead, one attempts modeling the behavior of the flow in the limit of very large Re. As the Kolmogorov assumption of self-similarity is known to be violated (e.g., by intermittency[6,7] and by spectral nonlocality[8]), the value of Re can play an important role; e.g., in the competition between two or more instabilities.[9] Therefore, another approach models the effects of turbulence at higher Reynolds numbers than are possible with a DNS on a given grid, by using a variety of techniques that can be viewed as filtering of the small scales [the so-called subgrid-scale (SGS) models].

[a)]Currently at Max-Planck-Institut für Sonnensystemforschung, 37191 Katlenburg-Lindau, Germany.

 © 2008 American Institute of Physics

Downloaded 17 Jun 2008 to 157.92.44.71. Redistribution subject to AIP license or copyright; see http://pof.aip.org/pof/copyright.jsp

A rather novel approach to modeling of turbulent flows employs *regularization modeling* as a SGS model.[10–15] Unlike closures that employ eddy-viscosity concepts (modifying the dissipative processes), the approach of regularization modeling modifies the spectral distribution of energy. For this reason, they retain a well-defined Reynolds number. Existence and uniqueness of smooth solutions can be rigorously proven, unlike many LES models (e.g., eddy-viscosity), as well as the fact that the subgrid model recovers the Navier–Stokes equations in the limit of the filter width going to zero. Their robust analytical properties ensure computability of solutions. These same properties reopen theoretical possibilities first explored by Leray when he proved the existence (but not smoothness or uniqueness) of solutions to the Navier–Stokes equations in Re^n $(n=2,3)$ using the Leray model.[16] This treatment of the small scales, then, enforces a precise type of regularization of the entire solution, which may be studied as an independent scientific question (as compared to either LES or SGS modeling).

Geurts and Holm[11,12,15] began using the Leray model with (a three-point invertible approximation of) an inverse-Helmholtz-operator filter of width α. Later it was dubbed Leray-α, and an upper bound for the dimension of the global attractor was established.[14] The global existence and uniqueness of strong solutions for the Leray model is a classical result.[16] Leray-α has been compared to DNS simulations on a grid of $N^3=192^3$ in a doubly periodic compressible channel flow domain.[11,12,15] Its performance was found to be superior to a dynamic mixed (similarity plus eddy-viscosity) model (with an even greater reduction in computational cost). However, it possessed a systematic error of a slight overprediction of the large scales accompanied by a slight underprediction of the small scales. It possessed both forward- and backscatter, but exhibited too little dissipation.

The Leonard tensor-diffusivity model[17] (sometimes known as the Clark model[18]) is the first term of the reconstruction series for the turbulent subfilter stress for all symmetric filters that possess a finite nonzero second moment. This leading order approximation of the subgrid stress is thus generic.[19,20] In *a priori* testing, it reconstructs a significant fraction ($>90\%$, but not all) of the subgrid stress, provides for local backscatter along the stretching directions while remaining globally dissipative, and possesses a better reconstruction of the subgrid stress than the scale-similarity model. Used as a LES, in *a posteriori* testing the Leonard tensor-diffusivity model required additional dissipation (a dynamic Smagorinsky term) to achieve reasonable gains in computation speed for three-dimensional (3D) periodic flows and for channel flows.[19] The Leonard tensor-diffusivity model does not conserve energy in the nonviscous limit. Cao, Holm, and Titi[21] developed a related (conservative) subgrid model that they dubbed Clark-α. The Clark-α model applies an additional inverse-Helmholtz filter operation to the Reynolds stress tensor of the Clark model. The global well-posedness of the Clark-α model and the existence and uniqueness of its solutions were demonstrated, and upper bounds for the Hausdorff (d_{H}) and fractal (d_F) dimensions of the global attractor were found.[21] This model has yet to be evaluated numerically.

The third regularization model we will consider is the incompressible Lagrangian-averaged Navier–Stokes (LANS-α, α-model, also known as the viscous Camassa–Holm equation[22–24,10,25]). It can be derived, for instance, by applying temporal averaging to Hamilton's principle, where Taylor's frozen-in turbulence hypothesis (the only approximation in the derivation) is applied as the closure for the Eulerian fluctuation velocity in the Reynold decomposition, at linear order in the generalized Lagrangian mean description.[26–28] In this derivation, the momentum-conservation structure of the equations is retained. For scales smaller than the filter width, LANS-α reduces the steepness in gradients of the Lagrangian mean velocity and thereby limits how thin the vortex tubes may become as they are transported, while the effect on larger length scales is negligible.[10] LANS-α may also be derived by smoothing the transport velocity of a material loop in Kelvin's circulation theorem.[29] Consequently, there is no attenuation of resolved circulation, which is important for many engineering and geophysical flows where accurate prediction of circulation is highly desirable. An alternative interpretation of the α-model is that it neglects fluctuations in the smoothed velocity field, while preserving them in the source term, the vorticity.[30]

LANS-α has previously been compared to direct numerical simulations (DNS) of the Navier–Stokes equations at modest Taylor Reynolds numbers ($\mathrm{Re}_\lambda \approx 72$,[31] $\mathrm{Re}_\lambda \approx 130$,[10] and $\mathrm{Re}_\lambda \approx 300$[14]). LANS-$\alpha$ was compared to a dynamic eddy-viscosity LES in 3D isotropic turbulence under two different forcing functions (for $\mathrm{Re}_\lambda \approx 80$ and 115) and for decaying turbulence with initial conditions peaked at a low wavenumber (with $\mathrm{Re}_\lambda \approx 70$) as well as at a moderate wavenumber (with $\mathrm{Re}_\lambda \approx 220$).[32] LANS-$\alpha$ was preferable in these comparisons because it demonstrated correct alignment between eigenvectors of the subgrid stress tensor and the eigenvectors of the resolved stress tensor and vorticity vector. The LES effectiveness of the LANS-α and the Leray-α regularization models relative to eddy-viscosity and the dynamic mixed model (similarity plus eddy-viscosity) have already been demonstrated in a turbulent mixing shear layer (with $\mathrm{Re} \approx 50$).[33,15] LANS-α was found to be the most accurate of these three LES candidates at proper subgrid resolution, but the effects of numerical contamination can be strong enough to lose most of this potential. While LANS-α has the greatest grid-independent accuracy of the three models, it also requires the greatest resolution. From the LES perspective, this could pose some limitations on the practical use and application of LANS-α for high Re cases. Indeed, recent high-resolution simulations of LANS-α showed that energy artificially accumulates in the subfilter scales, giving as a result only a modest computational gain at very high Reynolds number.[34]

We propose to pursue these previous studies of Leray-α and LANS-α further at higher Reynolds number, and to use them as a benchmark for evaluation of Clark-α. One goal is to contrast the subfilter-scale physics of the three models to determine the relevant features from which to build improved models. As the three regularizations are related via truncation of subfilter stresses, such a comparison can be illuminating. For LANS-α, the predicted subfilter-scale spec-

Downloaded 17 Jun 2008 to 157.92.44.71. Redistribution subject to AIP license or copyright; see http://pof.aip.org/pof/copyright.jsp

tra is $\sim k^{-1}$.[29] This scaling has been observed to be subdominant to an energy spectrum $\sim k^{1}$, which corresponds to "enslaved rigid body" or "polymerized" portions of the fluid.[34] The subfilter scaling observed in the third-order structure function corresponded to the predicted $\sim k^{-1}$ scaling of the energy spectrum. However, regions were observed in the flow where no stretching was acting in the subfilter scales. These regions, which give no contribution to the energy cascade, and hence do not affect the third-order structure functions, are responsible for the $\sim k^{1}$ scaling in the LANS-α energy spectrum. For Clark-α, the correct time scale for vortex stretching is difficult to determine and its spectrum is found to range between $\sim k^{-1}$ and $\sim k^{-7/3}$.[21] Leray-α has the same difficulty and the spectrum can range between $\sim k^{-1/3}$ and $\sim k^{-5/3}$.[14] The determination of these scaling laws is needed to quantify the computational gain if each model is to be used as a SGS model. As a result, we seek to determine empirically the subfilter-scale spectra. Our second goal is to evaluate the applicability of these three regularizations as SGS models. This is accomplished both through prediction of computational gains from observed subfilter-scale properties and through directly testing their capability to predict superfilter-scale properties at high Re.

We present the three models and describe how they are related, derive the de Kármán–Howarth equation for Clark-α and Leray-α (from which exact scaling laws for third order quantities follow), and review theoretical predictions of inertial range scaling in Sec. II. We examine the subfilter-scale properties of the three regularizations in Sec. III. We first compute a fully resolved DNS of the Navier–Stokes equations at a resolution of 1024^3 ($\nu=3\times10^{-4}$, $\mathrm{Re}\approx3300$, and $\mathrm{Re}_\lambda\approx790$). We then perform model runs with the exact same conditions at a resolution of 384^3. We take α to be $1/13$ the box size, which was found in an earlier study to be large enough to exhibit both Navier–Stokes and subfilter-scale LANS-α dynamics.[34] This large filter case is important because it gives insight into the behavior of the models at scales much smaller than the filter width without requiring higher resolution than is feasible. We compare the three regularizations as subgrid models in Sec. IV. Guided by a previous study of LANS-α,[34] we take α to be $1/40$ the box size. This choice was found to produce an optimal α-LES (in the sense of being optimal for the class of LANS-α models, with respect to the value of α). Finally, we review bounds on the size of the attractors and use these bounds to comment on the computational savings of the three regularizations viewed as SGS models.

II. THE THREE REGULARIZATION MODELS

A. Clark-α

The incompressible Navier–Stokes equations are given in Cartesian coordinates by

$$\partial_t v_i + \partial_j(v_j v_i) + \partial_i \mathcal{P} = \nu\partial_{jj} v_i, \quad \partial_i v_i = 0. \tag{1}$$

Filtering these equations with a convolution filter, $L: z\to\bar{z}$, in which $\bar{z}$ (z) denotes the filtered (unfiltered) field, yields

$$\partial_t u_i + \partial_j(u_j u_i) + \partial_i \bar{\mathcal{P}} + \partial_j \bar{\tau}_{ij} = \nu\partial_{jj} u_i, \tag{2}$$

in which by convention we denote $\underline{u_i}\equiv\bar{v}_i$ and the Reynolds turbulence stress tensor, i.e., $\bar{\tau}_{ij}=\overline{v_i v_j}-\bar{v}_i\bar{v}_j$, represents the closure problem. Equation (2) can represent *either* a LES or a SGS model. As the difference between the two is primarily philosophical (e.g., the scale at which filtering is applied, dissipative versus dispersive, the factor by which computational resolution may be decreased, etc.), we briefly define our terminology. Many LES include eddy-viscosity (i.e., $\partial_j\bar{\tau}_{ij}$ includes a $\nu_T\partial_{jj}u_i$ term such that $\nu_T\gg\nu$). This amounts to approximating the $\nu=0$ problem and no finite Reynolds number can be defined. More generally, a LES applies the filtering in the inertial range and reduces the necessary computational linear resolution by at least an order of magnitude. Different from this previous case, a SGS model employs a finite value of ν (and a well-defined Reynolds number) and addresses instead the question: For a given Re, how far can we reduce the computational expense while retaining as much of the detailed large-scale properties (such as the high-order statistics) as possible? For the case of LANS-α, for example, it has already been shown that the reduction in computational expense is rather modest (a factor of about 30). Therefore, while calling it a SGS model is justified by Eq. (2), the label LES does not really apply.

It is the case for both LES and SGS models that though a single filtering is indicated in Eq. (2), numerical solution implies a second filtering at the grid resolution (see, e.g., Ref. 20). Systematic studies requiring a database of computed solutions have been made in the past for LES[35] and for the LANS-α regularization model.[33,15,34] These studies show that the ratio of the two filter widths (i.e., the subfilter resolution) can affect greatly the model's performance. To avoid this complication, the subfilter resolutions employed in this study are rather large. Determination of the optimal subfilter resolution is a detailed study that should be undertaken for both Clark-α and Leray-α, but is beyond the scope of this present paper.

It has been shown[19,20] that for all symmetric filters possessing a finite nonzero second moment, the first term of the reconstruction series for the turbulent subfilter stress is

$$\bar{\tau}_{ij} = -\left.\frac{d^2\hat{G}}{dk^2}\right|_{k=0} \partial_k u_i \partial_k u_j + \cdots, \tag{3}$$

where $\hat{G}(k)$ is the Fourier transform of the convolution kernel $\{G(\mathbf{r})$ is the convolution kernel, where $[Lz](\mathbf{r})=\int G(\mathbf{r}-\mathbf{r}')z(\mathbf{r}')d^3\mathbf{r}'\}$. This approximation of the subgrid stress is then generic and is known as the Leonard tensor-diffusivity model[17] (or, often, the Clark model[18]). Related to this model, the Clark-α model is[21]

$$\partial_t v_i + \mathcal{H}\partial_j(u_j u_i) + \partial_i p + \alpha^2\partial_j(\partial_k u_i \partial_k u_j) = \nu\partial_{jj} v_i, \tag{4}$$

and its subgrid stress for $\alpha\ll1$ is given by

$$\bar{\tau}^C_{ij} = \mathcal{H}^{-1}\alpha^2(\partial_k u_i\partial_k u_j) = \alpha^2(\partial_k u_i\partial_k u_j) + \mathcal{O}(\alpha^4). \tag{5}$$

Here the filter is the inverse of a Helmholtz operator; i.e., $L=\mathcal{H}^{-1}=(1-\alpha^2\nabla^2)^{-1}$. The Clark-$\alpha$ model conserves energy in the $\mathcal{H}^1_\alpha(u)$ norm instead of the $L^2(v)$ norm,

Downloaded 17 Jun 2008 to 157.92.44.71. Redistribution subject to AIP license or copyright; see http://pof.aip.org/pof/copyright.jsp

$$\frac{dE_\alpha}{dt} = -2\nu\Omega_\alpha, \tag{6}$$

in which the Clark-α energy E_α is expressed as

$$E_\alpha = \frac{1}{D}\int_D \frac{1}{2}(\mathbf{u} - \alpha^2\nabla^2\mathbf{u})\cdot\mathbf{u}d^3x = \frac{1}{D}\int_D \frac{1}{2}\mathbf{v}\cdot\mathbf{u}d^3x, \tag{7}$$

and the Clark-α energy dissipation rate is given by

$$\Omega_\alpha = \frac{1}{D}\int_D \frac{1}{2}\boldsymbol{\omega}\cdot\bar{\boldsymbol{\omega}}d^3x, \tag{8}$$

where $\boldsymbol{\omega}=\nabla\times\mathbf{v}$ and $\bar{\boldsymbol{\omega}}=\nabla\times\mathbf{u}$. For $L=\mathcal{H}^{-1}$, we note that $\hat{G}=(1+\alpha^2k^2)^{-1}$, which implies that the turbulent subfilter stress tensor for the tensor-diffusivity model given by Eq. (3) is

$$\bar{\tau}_{ij}^C = 2\alpha^2(\partial_k u_i \partial_k u_j) + \cdots, \tag{9}$$

which is proportional to the Clark-α stress tensor to second order in α. Hence, the *a priori* tests of[19] should apply to Clark-α, at least at this order.

1. de Kármán–Howarth equation for Clark-α

In 1938, de Kármán and Howarth[36] introduced the invariant theory of isotropic hydrodynamic turbulence, and derived from the Navier–Stokes equations the exact law relating the time derivative of the two-point velocity correlation to the divergence of the third-order correlation function. The corresponding de Kármán–Howarth theorem for LANS-α in the fluid case was derived in Ref. 37. The relevance of the de Kármán–Howarth theorem for the study of turbulence cannot be underestimated. As a corollary, rigorous scaling laws in the inertial range can be deduced. In this section, we derive these results for the Clark-α case.

For the sake of simplicity, we consider the case $\nu=0$, since the dissipative terms may be added at any point in the derivation. We denote $\mathbf{u}'\equiv\mathbf{u}(\mathbf{x}',t)$ and begin our investigation of the correlation dynamics by computing the ingredients of the partial derivative $\partial_t(v_i u_j')$. The Clark-α motion equation (4) may be rewritten as

$$\partial_t v_i + \partial_m(v_i u_m + u_i v_m - u_i u_m + p\,\delta_{im} - \alpha^2\partial_n u_i \partial_n u_m) = 0. \tag{10}$$

Combining Eqs. (2) and (5), we arrive at the fluctuation-velocity equation

$$\partial_t u_j' + \partial_m'(u_j' u_m' + \bar{p}'\,\delta_{jm} + \alpha^2 G\otimes\tau_{jm}^{C'}) = 0, \tag{11}$$

where $\bar{\tau}_{ij}^C \equiv \mathcal{H}^{-1}\alpha^2\tau_{ij}^C$ $(L=\mathcal{H}^{-1})$. Multiplying Eq. (10) by u_j' and Eq. (11) by v_i, then adding the result yields

$$\partial_t\langle v_i u_j'\rangle = \frac{\partial}{\partial r_m}\langle(v_i u_m + u_i v_m - u_i u_m - \alpha^2\partial_n u_i\partial_n u_m)u_j'\rangle + \frac{\partial}{\partial r_m}\langle p u_j'\delta_{im} - \bar{p}' v_i\delta_{jm}\rangle - \frac{\partial}{\partial r_m}\langle(u_j' u_m' + \alpha^2 G\otimes\tau_{jm}^{C'})v_i\rangle, \tag{12}$$

where we have used statistical homogeneity

$$\frac{\partial}{\partial r_m}\langle\cdot\rangle = \frac{\partial}{\partial x_m'}\langle\cdot\rangle = -\frac{\partial}{\partial x_m}\langle\cdot\rangle. \tag{13}$$

We symmetrize Eq. (12) in the indices i, j by adding the corresponding equation for $\partial_t\langle v_j u_i'\rangle$. We then use homogeneity again as

$$\langle v_i u_j' u_m' + v_j u_i' u_m'\rangle = -\langle v_i' u_j u_m + v_j' u_i u_m\rangle, \tag{14}$$

and define the tensors

$$\mathcal{Q}_{ij}^C = \langle v_i u_j' + v_j u_i'\rangle, \tag{15}$$

$$\mathcal{T}_{ijm}^C = \langle(v_i u_j' + v_j u_i' + v_i' u_j + v_j' u_i - u_i u_j' - u_j u_i')u_m + (u_i u_j' + u_j u_i')v_m\rangle, \tag{16}$$

$$\Pi_{ijm}^C = \langle(p u_j' - \bar{p}' v_j)\delta_{im} + (p u_i' - \bar{p}' v_i)\delta_{jm}\rangle, \tag{17}$$

$$\mathcal{S}_{ijm}^C = \langle(\partial_n u_i\partial_n u_m)u_j' + (\partial_n u_j\partial_n u_m)u_i' + G\otimes\tau_{jm}^{C'}v_i + G\otimes\tau_{im}^{C'}v_j\rangle. \tag{18}$$

We can drop Π_{ijm}^C because the terms with the pressures p and $\bar{p}'$ vanish everywhere, as follows from the arguments of isotropy.[36] Finally, we obtain

$$\partial_t\mathcal{Q}_{ij}^C = \frac{\partial}{\partial r_m}(\mathcal{T}_{ijm}^C - \alpha^2\mathcal{S}_{ijm}^C). \tag{19}$$

This is the de Kármán–Howarth equation for Clark-α [compare to Eq. (3.8) in Ref. 37 for LANS-α].

By dimensional analysis, the energy dissipation rate in Clark-α is $\epsilon_\alpha^C \sim \partial_t\mathcal{Q}^C{}_{ij}$ and Eq. (19) implies

$$\varepsilon_\alpha^C \sim \frac{1}{l}\left(vu^2 + u^3 + \frac{\alpha^2}{l^2}u^3\right). \tag{20}$$

For large scales $(l \gg \alpha)$, we recover the Navier–Stokes scaling known as the four-fifths law: $\langle[\delta v_\parallel(l)]^3\rangle \sim \varepsilon l$.[1] Here, $\delta v_\parallel(l)\equiv[\mathbf{v}(\mathbf{x}+l)-\mathbf{v}(\mathbf{x})]\cdot\mathbf{l}/l$ is the longitudinal increment of $\mathbf{v}$. Strictly speaking, the four-fifths law expresses that the third-order longitudinal structure function of $\mathbf{v}$, i.e., $S_3^v(l)\equiv\langle(\delta v_\parallel)^3\rangle$, is given in the inertial range in terms of the mean energy dissipation per unit mass ε by

$$S_3^v = -\tfrac{4}{5}\varepsilon l, \tag{21}$$

or, equivalently, that the flux of energy across scales in the inertial range is constant. We also recover the Kolmogorov 1941[2–4] (hereafter, K41) energy spectrum, i.e., $E(k)k \sim v^2 \sim \varepsilon^{2/3}l^{2/3}$ or, equivalently,

Downloaded 17 Jun 2008 to 157.92.44.71. Redistribution subject to AIP license or copyright; see http://pof.aip.org/pof/copyright.jsp

$$E(k) \sim \varepsilon^{2/3} k^{-5/3}. \tag{22}$$

For subfilter scales ($l \ll \alpha$), we have $u \sim v l^2/\alpha^2$ and the first and third right-hand terms in Eq. (20) are equivalent. In this case, we are left with two different possible scalings depending on the prefactors in Eq. (20). If the first (or third) right-hand term is dominant, our scaling law becomes

$$\langle (\delta u_{\parallel}(l))^2 (\delta v_{\parallel}(l)) \rangle \sim \varepsilon_{\alpha}^{C} l. \tag{23}$$

For our subfilter-scale energy spectrum, we would then have $E_{\alpha}^{C}(k)k \sim uv \sim (\varepsilon_{\alpha}^{C})^{2/3}\alpha^{2/3}$, or, equivalently,

$$E_{\alpha}^{C}(k) \sim (\varepsilon_{\alpha}^{C})^{2/3}\alpha^{2/3}k^{-1}. \tag{24}$$

This result is the same as for the α-model.[29] If, however, the second right-hand term in Eq. (20) is dominant, then the K41 results are recovered, with **u** substituted for **v**. In that case, one finds the alternative Clark-α subfilter-scale spectral energy scaling,

$$E_{\alpha}^{C}(k) \sim k^{1/3}. \tag{25}$$

2. Phenomenological arguments for Clark-α inertial range scaling

We review here the derivation by dimensional analysis of the spectrum which follows the scaling ideas originally due to Kraichnan[38] and which is developed more fully in Ref. 21. In examining the nonlinear terms in Eq. (4), it is not entirely clear which of three possible scales for the average velocity for an eddy of size k^{-1},

$$U_k^{(0)} = \left(\frac{1}{D} \int_D |\mathbf{v}_k|^2 d^3x \right)^{1/2}, \tag{26}$$

$$U_k^{(1)} = \left(\frac{1}{D} \int_D \mathbf{u}_k \cdot \mathbf{v}_k d^3x \right)^{1/2}, \tag{27}$$

or

$$U_k^{(2)} = \left(\frac{1}{D} \int_D |\mathbf{u}_k|^2 d^3x \right)^{1/2}, \tag{28}$$

should result. Therefore, three corresponding "turnover times" $\mathfrak{t}_k$ for such an eddy may be proposed,

$$\mathfrak{t}_k^{(n)} \sim 1/(kU_k^{(n)}) \quad \text{with } n = 0,1,2. \tag{29}$$

The term "turnover time" is used advisedly here, since only the velocity $U_k^{(2)}$ is composed of the fluid transport velocity. We define the (omnidirectional) spectral energy density $E_{\alpha}(k)$ from the relation

$$E_{\alpha} = \int_0^{\infty} \oint E_{\alpha}(\mathbf{k}) d\sigma d\mathbf{k} = \int_0^{\infty} E_{\alpha}(k) dk. \tag{30}$$

Since $\mathbf{u}_k \cdot \mathbf{u}_k = \mathbf{u}_k \cdot \mathbf{v}_k/(1+\alpha^2k^2) = E_{\alpha}(k)/(1+\alpha^2k^2)$, we have

$$U_k^{(n)} \sim \left(\int E_{\alpha}(k)(1+\alpha^2k^2)^{(1-n)} dk \right)^{1/2} \sim \left[kE_{\alpha}(k)(1+\alpha^2k^2)^{(1-n)} \right]^{1/2}. \tag{31}$$

The total energy dissipation rate ε_{α}^{C} is then related to the spectral energy density by

$$\varepsilon_{\alpha} \sim \left[\mathfrak{t}_k^{(n)} \right]^{-1} \int E_{\alpha}(k) dk \sim k^2 U_k^{(n)} E_{\alpha}(k) \sim k^{5/2} E_{\alpha}^{C}(k)^{3/2} (1+\alpha^2k^2)^{(1-n)/2}, \tag{32}$$

which yields, finally, the predicted energy spectra for Clark-α, $E_{\alpha}^{C}(k)$,

$$E_{\alpha}^{C}(k) \sim (\varepsilon_{\alpha}^{C})^{2/3} k^{-5/3} (1+\alpha^2k^2)^{(n-1)/3}. \tag{33}$$

For scales much larger than α ($\alpha k \ll 1$), the Kolmogorov scaling for Navier–Stokes is recovered,

$$E_{\alpha}^{C}(k) \sim (\varepsilon_{\alpha}^{C})^{2/3} k^{-5/3}, \tag{34}$$

whereas for scales much smaller ($\alpha k \gg 1$), the spectrum becomes

$$E_{\alpha}^{C}(k) \sim (\varepsilon_{\alpha}^{C})^{2/3} \alpha^{2(n-1)/3} k^{(2n-7)/3}. \tag{35}$$

These arguments constrain the Clark-α subfilter-scale spectrum to lie between k^{-1} and $k^{-7/3}$.

B. Leray-α

The Leray model in Cartesian coordinates is

$$\partial_t v_i + \partial_j (u_j v_i) + \partial_i P = \nu \partial_{jj} v_i \quad \partial_i v_i = 0, \tag{36}$$

where the flow is advected by a smoothed velocity **u**. By comparison with Eq. (2) we see that the Leray model approximates the subgrid stress as $\bar{\tau}_{ij}^{\mathrm{L}} = L(u_j v_i) - u_j u_i$, or, with $L = \mathcal{H}^{-1}$,

$$\bar{\tau}_{ij}^{\mathrm{L}} = \mathcal{H}^{-1} \alpha^2 (\partial_k u_i \partial_k u_j + \partial_k u_i \partial_j u_k). \tag{37}$$

As has been noted previously,[13] the subgrid stress of Clark-α in Eq. (5) is a truncation of the subgrid stress of Leray-α, in Eq. (37). For Leray-α, the $L^2(v)$ norm is the quadratic invariant that is identified with energy,

$$\frac{dE}{dt} = -2\nu\Omega, \tag{38}$$

where

$$E = \frac{1}{D} \int_D \frac{1}{2} |\mathbf{v}|^2 d^3x \tag{39}$$

and

$$\Omega = \frac{1}{D} \int_D \frac{1}{2} |\boldsymbol{\omega}|^2 d^3x. \tag{40}$$

As was pointed out in Ref. 39, the incompressibility of the velocity field **v** only implies a divergenceless filtered velocity **u** under certain boundary conditions for Leray-α. When $\partial_i u_i \neq 0$, the energy $E = \frac{1}{2}\int_D |\mathbf{v}|^2$ is no longer conserved (helicity and Kelvin's theorem are not conserved for Leray-α). In our numerical study, we employ periodic boundary condi-

Downloaded 17 Jun 2008 to 157.92.44.71. Redistribution subject to AIP license or copyright; see http://pof.aip.org/pof/copyright.jsp

tions, for which $\partial_i v_i = 0$ implies $\partial_i u_i = 0$ and Leray-α conserves energy in the usual sense of $L^2(v)$.

1. de Kármán–Howarth equation for Leray-α

In this section we derive the de Kármán–Howarth equation for the Leray-α case. Following Sec. II A 1, we begin our investigation of the correlation dynamics by computing the ingredients of the partial derivative $\partial_t(v_i v_j')$. Equation (36) may be rewritten as

$$\partial_t v_i + \partial_m(v_i u_m + P\delta_{im}) = 0. \tag{41}$$

Multiplying Eq. (41) by v_j' yields

$$\partial_t \langle v_i v_j' \rangle = \frac{\partial}{\partial r_m}\langle v_i u_m v_j' \rangle + \frac{\partial}{\partial r_m}\langle P v_j' \delta_{im} \rangle. \tag{42}$$

We can make this equation symmetric in the indices i, j, by adding the equation for $\partial_t \langle v_j v_i' \rangle$. We define the tensors

$$\mathcal{Q}_{ij}^{\mathrm{L}} = \langle v_i v_j' + v_j v_i' \rangle, \tag{43}$$

$$\mathcal{T}_{ijm}^{\mathrm{L}} = \langle (v_i v_j' + v_j v_i') u_m \rangle, \tag{44}$$

$$\Pi_{ijm}^{\mathrm{L}} = \langle P v_j' \delta_{im} + P v_i' \delta_{jm} \rangle. \tag{45}$$

Again, we may drop Π_{ijm}^{L} because the terms with the pressure P vanish everywhere, and thereby obtain

$$\partial_t \mathcal{Q}_{ij}^{\mathrm{L}} = \frac{\partial}{\partial r_m}\mathcal{T}_{ijm}^{\mathrm{L}}. \tag{46}$$

This is the de Kármán–Howarth equation for Leray-α.

The energy dissipation rate for Leray-α is denoted by ε^{L}, and it satisfies $\varepsilon^{\mathrm{L}} \sim \partial_t \mathcal{Q}_{ij}^{\mathrm{L}}$. By dimensional analysis, Eq. (46) implies

$$\varepsilon^{\mathrm{L}} \sim \frac{1}{l} v^2 u. \tag{47}$$

For large scales ($l \gg \alpha$), we recover the Navier–Stokes scaling [Eqs. (21) and (22)]. For subfilter scales ($l \ll \alpha$), our scaling law becomes

$$\langle [\delta v_{\parallel}(l)]^2 [\delta u_{\parallel}(l)] \rangle \sim \varepsilon^{\mathrm{L}} l. \tag{48}$$

For our small-scale energy spectrum, we would then have $E^{\mathrm{L}}(k)k \sim v^2 \sim (\varepsilon^{\mathrm{L}})^{2/3}\alpha^{4/3}k^{2/3}$ (where we employed $u \sim v l^2/\alpha^2$), or, equivalently [cf. Eq. (25)],

$$E^{\mathrm{L}}(k) \sim (\varepsilon^{\mathrm{L}})^{2/3}\alpha^{4/3}k^{-1/3}. \tag{49}$$

2. Phenomenological arguments for Leray-α inertial range scaling

We review here the derivation by dimensional analysis of the spectrum for Leray-α as we did for Clark-α in Sec. II A 2. This analysis is developed more fully in Ref. 14. We argue again that there are three possible scales for the average velocity for an eddy of size k^{-1} [Eqs. (26)–(28)], with the turnover time $\mathrm{t}_k^{(n)}$ given by Eq. (29). Since $u_k^2 = v_k^2/(1+\alpha^2k^2)^2 = E(k)/(1+\alpha^2k^2)^2$, we have

$$(U_k^{(n)}) \sim \left(\int E(k)(1+\alpha^2k^2)^{-n} dk \right)^{1/2} \sim (kE(k)(1+\alpha^2k^2)^{-n})^{1/2}, \tag{50}$$

Then, the total energy dissipation rate ε^{L} is then related to the spectral energy density by

$$\varepsilon^{\mathrm{L}} \sim (\mathrm{t}_k^{(n)})^{-1} \int E(k)dk \sim k^2 U_k^{(n)} E(k) \sim k^{5/2}E(k)^{3/2}(1+\alpha^2k^2)^{-n/2}, \tag{51}$$

which yields, finally, the predicted energy spectra for Leray-α, $E^{\mathrm{L}}(k)$,

$$E^{\mathrm{L}}(k) \sim (\varepsilon^{\mathrm{L}})^{2/3}k^{-5/3}(1+\alpha^2k^2)^{n/3}. \tag{52}$$

For scales much larger than α ($\alpha k \ll 1$), the K41 spectrum is recovered [Eq. (22)], and for scales much smaller ($\alpha k \gg 1$), the spectrum is

$$E^{\mathrm{L}}(k) \sim (\varepsilon^{\mathrm{L}})^{2/3}\alpha^{2n/3}k^{(2n-5)/3}. \tag{53}$$

These arguments constrain the Leray-α subfilter-scale spectrum to lie between $k^{-1/3}$ and $k^{-5/3}$.

C. LANS-α

LANS-α is given by

$$\partial_t v_i + \partial_j(u_j v_i) + \partial_i \pi + v_j \partial_i u_j = \nu \partial_{jj} v_i, \quad \partial_i v_i = 0. \tag{54}$$

For LANS-α, the usual choice of filter is again $L = \mathcal{H}^{-1}$. With this filter, the subgrid stress tensor is given by

$$\overline{\tau}_{ij}^{\alpha} = \mathcal{H}^{-1}\alpha^2(\partial_m u_i \partial_m u_j + \partial_m u_i \partial_j u_m - \partial_i u_m \partial_j u_m). \tag{55}$$

As has been previously noted,[13] the subgrid stress of Leray-α, Eq. (37), is a truncation of the subgrid stress of LANS-α equation (55). Like Clark-α, energy is conserved in the $H_\alpha^1(u)$ norm instead of the $L^2(v)$ norm. Additionally, LANS-α is the only model of the three examined here that conserves a form of the helicity (and Kelvin's circulation theorem).

For LANS-α in the fluid case the de Kármán–Howarth theorem was derived in Ref. 37. We summarize here the dimensional analysis argument for the LANS-α inertial range scaling that follows from this theorem, beginning from Eq. (3.8) in Ref. 37. In the statistically isotropic and homogeneous case, without external forces and with $\nu = 0$, taking the dot product of Eq. (54) with u_j' yields the equation

$$\partial_t \mathcal{Q}_{ij}^{\alpha} = \frac{\partial}{\partial r_m}(\mathcal{T}_{ijm}^{\alpha} - \alpha^2 \mathcal{S}_{ijm}^{\alpha}). \tag{56}$$

The trace of this equation is the Fourier transform of the detailed energy balance for LANS-α;

$$\mathcal{Q}_{ij}^{\alpha} = \langle v_i u_j' + v_j u_i' \rangle \tag{57}$$

is the second-order correlation tensor, while

$$\mathcal{T}_{ijm}^{\alpha} = \langle (v_i u_j' + v_j u_i' + v_i' u_j + v_j' u_i) u_m \rangle \tag{58}$$

and

Downloaded 17 Jun 2008 to 157.92.44.71. Redistribution subject to AIP license or copyright; see http://pof.aip.org/pof/copyright.jsp

$$\mathcal{S}^{\alpha}_{ijm} = \langle (\partial_m u_l \partial_i u_l) u'_j + (\partial_m u_l \partial_j u_l) u'_i + (G \otimes \tau^{\alpha\prime}_{jm}) v_i + (G \otimes \tau^{\alpha\prime}_{im}) v_j \rangle \tag{59}$$

are the third-order correlation tensors for LANS-α and $\bar{\tau}^{\alpha}_{ij} = \mathcal{H}^{-1}\alpha^2 \tau^{\alpha}_{ij}$ is the subfilter-scale stress tensor. For $\alpha = 0$ this reduces to the well-known relation derived by de Kármán and Howarth. The energy dissipation rate for LANS-α, i.e., ε_α, satisfies $\varepsilon_\alpha \propto \partial_l \mathcal{Q}^{\alpha}_{ij}$. By dimensional analysis in Eq. (56) we arrive at

$$\varepsilon_\alpha \sim \frac{1}{l}\left(v u^2 + \frac{\alpha^2}{l^2} u^3 \right). \tag{60}$$

For large scales ($l \gg \alpha$), we recover the Navier–Stokes scaling equations (21) and (22). For subfilter scales ($l \ll \alpha$) our scaling law becomes Eq. (23) and our subfilter-scale spectra are given by

$$E_\alpha(k) \sim \varepsilon_\alpha^{2/3} \alpha^{2/3} k^{-1}. \tag{61}$$

In this case, by the phenomenological arguments, we know that eddies of size k^{-1} are advected by the smoothed velocity [Eq. (28)]. This scaling is confirmed in Ref. 34, but it coexists with a k^1 energy spectrum corresponding to "enslaved rigid bodies" or "polymerized" portions of fluid that do not contribute to the turbulent energy cascade.

III. SUBFILTER-SCALE PHYSICS

Only by examining the subfilter scales can we hope to derive new, improved models, and, ultimately, to gain an understanding of turbulence. A knowledge of the differences between closures and Navier–Stokes is fundamental to enable the derivation of better physical models of turbulence at small scales. In this section, then, we will be interested in both the similarities and the differences between the regularizations and Navier–Stokes. A more immediate goal of predicting the computational savings at higher Reynolds numbers can be achieved through the correct prediction of the scaling at small scales.

To this end, we compute numerical solutions to Eqs. (1), (4), (36), and (54) in a three-dimensional (3D) cube with periodic boundary conditions using a parallel pseudospectral code.[40,41] We employ a Taylor–Green forcing,[42]

$$F = \begin{bmatrix} \sin k_0 x \cos k_0 y \cos k_0 z \\ -\cos k_0 x \sin k_0 y \cos k_0 z \\ 0 \end{bmatrix} \tag{62}$$

(with $k_0 = 2$), and employ dynamic control[43] to maintain a nearly constant energy with time. The Taylor–Green forcing [Eq. (62)] is not a solution of the Euler's equations, and as a result small scales are generated rapidly. The resulting flow models the fluid between counter-rotating cylinders[44] and it has been widely used to study turbulence, including studies in the context of the generation of magnetic fields through dynamo instability.[45] We define the Taylor microscale as $\lambda = 2\pi\sqrt{\langle v^2 \rangle / \langle \omega^2 \rangle}$, and the mean velocity fluctuation as $v_{\rm rms} = [2\int_0^\infty E(k) dk^{1/2}$. The Taylor microscale Reynolds number is defined by $\mathrm{Re}_\lambda = v_{\rm rms}\lambda/\nu$ and the Reynolds number based on a unit length is $\mathrm{Re} = v_{\rm rms}/\nu$.

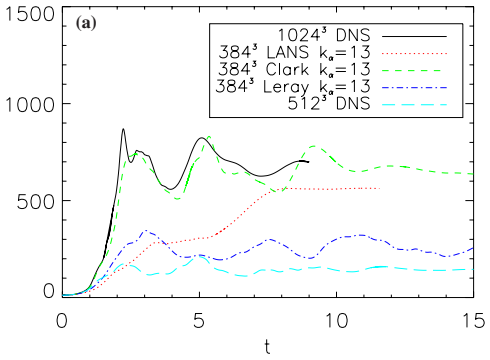

FIG. 1. (Color online) Time evolution of the enstrophy ($\langle \omega^2 \rangle$ for Leray-α and in the DNS, $\langle \boldsymbol{\omega} \cdot \bar{\boldsymbol{\omega}} \rangle$ for LANS-α and Clark-α). DNS ($\mathrm{Re} \approx 3300$) is shown as solid black lines, LANS-α as dotted red, Clark-α as dashed green, and Leray-α as blue dash-dotted. The cyan long-dashed line represents a 512^3 DNS ($\mathrm{Re} \approx 1300$, $\mathrm{Re}_\lambda \approx 490$). Here each run is calculated only until it reaches a statistical steady state. Leray-α reduces the dissipation, $\varepsilon = \nu\langle \omega^2 \rangle$, and increases the time scale to reach a statistical turbulent steady state. Both effects are greater as α is increased. By comparison with the $\mathrm{Re} \approx 1300$ run, we see that these two effects are consistent with a reduced effective Reynolds number. A smaller reduction in flux (but not an increase in time to steady state) is also observed for LANS-α and is likely related to its rigid bodies.

The Clark-α, Leray-α, and LANS-α equations (as well as other SGS models based on spectral filters) are easy to implement in spectral or pseudospectral methods. As an example, in Fourier based pseudospectral methods, the Helmholtz differential operator can be inverted to obtain $\hat{\mathcal{H}}^{-1}(k) = (1 + \alpha^2 k^2)^{-1}$, where the hat denotes Fourier transformed. In this way, the filter reduces to an algebraic operation, and Eqs. (4), (36), and (54) can be solved numerically at almost no extra cost. If other numerical methods are used, the inversion can be circumvented for example by expanding the inverse of the Helmholtz operator into higher orders of the Laplacian operator.[31,46]

To compare the three regularizations (Clark-α, Leray-α, LANS-α) we compute a fully resolved DNS of the Navier–Stokes equations at a resolution of 1024^3 ($\nu = 3 \times 10^{-4}$, $\mathrm{Re} \approx 3300$) and model runs with the exact same conditions at a resolution of 384^3. The details of the flow dynamics of the DNS have already been given.[8,47] In particular, the Reynolds number based on the integral scale $\mathfrak{L} \equiv 2\pi \int E(k) k^{-1} dk / E \approx 1.2$ (where E is the total energy) is $\mathrm{Re}_\mathfrak{L} = U\mathfrak{L}/\nu \approx 3900$, where U is the rms velocity and the Reynolds number based on the Taylor scale is $\mathrm{Re}_\lambda \approx 790$. The DNS was run for nine turnover times ($\mathfrak{L}/U$) (in the following results, time t is in units of the turnover time). We employ a filter width of $\alpha = 2\pi/13$ for which LANS-α exhibits both Navier–Stokes and LANS-α inertial ranges in the third-order structure function.[34] From these we hope to obtain the behavior of the models for scales much smaller than α

In Fig. 1, we present the time evolution of the enstrophy ($\langle \omega^2 \rangle$ for Leray-α and DNS; $\langle \boldsymbol{\omega} \cdot \bar{\boldsymbol{\omega}} \rangle$ for LANS-α and Clark-α), which is proportional to the dissipation ($\varepsilon = \nu\langle \omega^2 \rangle$ or $\varepsilon_\alpha = \nu\langle \boldsymbol{\omega} \cdot \bar{\boldsymbol{\omega}} \rangle$ depending on the case). Also shown is a well-resolved 512^3 DNS of a less turbulent flow [$\nu = 1.5 \times 10^{-3}$, $\mathrm{Re} \approx 1300$, $\mathrm{Re}_\lambda \approx 490$ (cyan online) long-dashed line]. Here, each run is calculated only until it reaches a

Downloaded 17 Jun 2008 to 157.92.44.71. Redistribution subject to AIP license or copyright; see http://pof.aip.org/pof/copyright.jsp

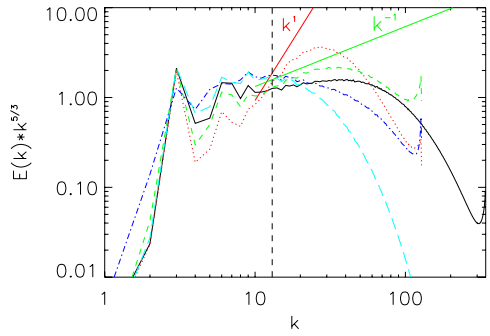

FIG. 2. (Color online) Spectra compensated by K41 for 1024^3 DNS ($\mathrm{Re}\approx 3300$) averaged over $t=[8.25,9]$. Labels are as in Fig. 1. The vertical dashed line indicates $k_\alpha \equiv 2\pi/\alpha$. Compensated spectra for 384^3 LANS-α averaged over $t\in[10.8,11.6]$, for 384^3 Clark-α over $t\in[11.8,12.6]$, for 384^3 Leray-α over $t\in[26.3,27]$, and for the $\mathrm{Re}\approx 1300$ DNS over $t\in[18.1,18.9]$. Due to the large disparity in times to reach a turbulent steady state, the time intervals chosen to average over also differ greatly. Clark-α approximates the predicted k^{-1} spectrum [Eq. (24)] and not $k^{1/3}$ [Eq. (25)] nor other possible spectra [Eq. (33)]. The spectrum of Leray-α is very similar (for $k\in[5,20]$) to that of the $\mathrm{Re}\approx 1300$ DNS. The positive but shallower than k^1 LANS-α spectrum observed here has previously been reported (see text). The spectra of all three regularizations clearly differ from that of Navier–Stokes.

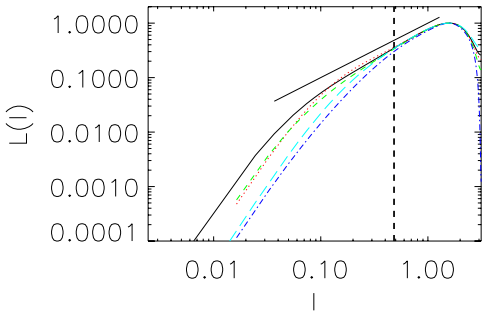

FIG. 3. (Color online) Third-order structure function associated with the de Kármán–Howarth equation $L^{(\alpha,\mathrm{L})}(l)$ vs length l. Labels are as in Fig. 1. The vertical dashed lines indicate the length α. The Clark-α result is consistent with a $u^2v\sim l^1$ scaling [Eq. (23)], and clearly inconsistent with a $u^2v\sim l^{-1}$ ($u^3\sim l$) scaling as would arise from the middle term in Eq. (20). The results for Leray-α are again consistent with a reduced effective Re.

statistically steady state. We see that the dissipation is greatly reduced and the time scale to reach a statistically steady state is increased for Leray-α. We see by comparison with the $\mathrm{Re}\approx 1300$ DNS that this reduced dissipation could result from a reduced effective Reynolds number in the Leray-α run. For LANS-α, the dissipation is decreased although the time to reach steady state is not increased. This is probably related to the enslavement of its rigid body regions which would have no internal dissipation. Of the three models, Clark-α most resembles the total dissipation for a large range of α. Indeed, as it is the order α^2 approximation of Navier–Stokes, this dissipation behavior for Clark-α may continue to hold until α becomes quite large.

Figure 2 shows a comparison of the energy spectrum at the turbulent steady state, for all the runs in Fig. 1. The isotropic energy spectra are calculated as follows:

$$E(k)=\sum_{k_{\mathrm{eff}}\geqslant k-1/2}^{k_{\mathrm{eff}}<k+1/2} v_x^2(k_{\mathrm{eff}})+v_y^2(k_{\mathrm{eff}})+v_z^2(k_{\mathrm{eff}}), \tag{63}$$

where $k_{\mathrm{eff}}=\sqrt{k_x^2+k_y^2+k_z^2}$ [the $H_1^\alpha(u)$ norm is employed for Clark-α and LANS-α]. The length scale α is indicated by a vertical dashed line and the plotted energy spectra are compensated by $k^{5/3}$ (i.e., leading to a flat K41 $k^{-5/3}$ spectrum). The energy flux in the DNS is constant in a wide range of scales, but the compensated spectrum has a more complex structure. The salient features of this spectrum are well known from previous studies.[6] Small scales before the dissipative range show the so-called bottleneck effect with a slope shallower than $k^{-5/3}$. On the other hand, larger scales have a tendency to develop a spectrum slightly steeper than $k^{-5/3}$ because of intermittency corrections, an effect that becomes clear in the simulation performed at larger spatial resolution on a grid of 4096^3 points.[6] From Fig. 2 it is clear that the Clark-α spectral behavior is close to the predicted k^{-1} spectrum, rather than the $k^{1/3}$ from Eq. (25), or the other possible spectra from Eq. (33). Likewise, the positive $k^{0.2}$ LANS-α spectrum observed here approaches k^1 with increasing resolution as the subfilter scales are fully resolved.[34] Leray-α, on the other hand, possesses a very steep subfilter-scale spectrum as well as enhanced large-scale energy as has been previously observed.[15] The results indicate that solutions to Leray-α are the most strongly regularized of the three regularizations.

The spectrum of Leray-α in Fig. 2 gives a good approximation to the $\mathrm{Re}\approx 1300$ DNS in the range $k\in[5,20]$ (i.e., to $\nu=1.5\times10^{-3}$ rather than to $\nu=3\times10^{-4}$, which was employed). This result, Leray-α's increased characteristic time scales, and its reduced dissipation, imply that the Leray-α model is operating at a much lower effective Reynolds number. This is also clear from the rapid drop in the spectrum at small scales, shown in Fig. 2. Indeed, we can build an effective Reynolds number in the large scales as $\mathrm{Re}_{\mathrm{eff}}=\epsilon^{1/3}\mathfrak{L}^{4/3}/\nu$. Since $\mathfrak{L}$ is controlled in this simulation by the forcing scale, the drop in the dissipation rate implies a reduced nonlinearity in Leray-α. This is also consistent with a direct comparison of the nonlinear terms in Leray-α with, for instance, LANS-α. The nonlinear terms in LANS-α [Eq. (54)] may be written as $\mathbf{u}\cdot\nabla\mathbf{v}+\nabla\mathbf{u}^T\cdot\mathbf{v}$ (where the suffix T denotes a transposition), while the nonlinear term in Leray-α [Eq. (36)] is only $\mathbf{u}\cdot\nabla\mathbf{v}$. Both nonlinear terms in LANS-α are of order $O(1)$, so the absence of one of the nonlinear terms in Leray-α could be understood as a reduction in the nonlinearity.

Validation of the de Kármán–Howarth equation scalings [Eqs. (23) and (48)] enables us to measure scaling laws in the inertial range and, thus, compare the intermittency properties of the models. The third-order correlations involved in the theorems, namely,

$$L^\alpha(l)\equiv\langle[\delta u_\parallel(l)]^2[\delta v_\parallel(l)]\rangle \tag{64}$$

for Clark-α and LANS-α,

$$L^{\mathrm{L}}(l)\equiv\langle[\delta v_\parallel(l)]^2[\delta u_\parallel(l)]\rangle \tag{65}$$

for Leray-α, and $L(l)\equiv S_3^v(l)$ for Navier–Stokes, are plotted versus l in Fig. 3. In Fig. 3 we can see validation of the de

Downloaded 17 Jun 2008 to 157.92.44.71. Redistribution subject to AIP license or copyright; see http://pof.aip.org/pof/copyright.jsp

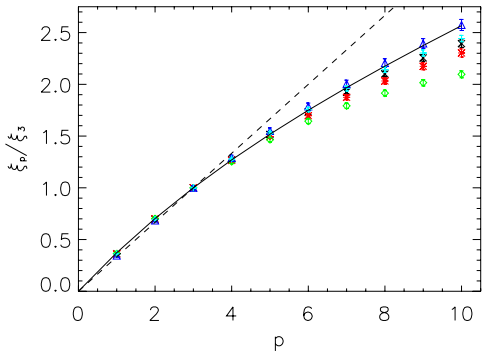

FIG. 4. (Color online) Normalized structure function scaling exponent ξ_p/ξ_3 vs order p. The dashed line indicates K41 scaling and the solid line the She–Lévêque formula (Ref. 53). The DNS results are indicated by black X's, LANS-α by red asterisks, Clark-α by green diamonds, Leray-α by blue triangles, and the Re$\approx$1300 DNS results are shown by cyan pluses. Leray-α is less intermittent consistent with the smoother field produced by a lower Re flow. Clark-α is more intermittent than Navier–Stokes at subfilter scales. LANS-α is less intermittent than Clark-α, likely due to the influence of its rigid bodies (see text).

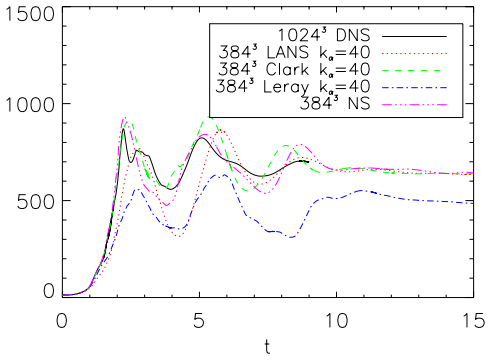

FIG. 5. (Color online) Time evolution of the enstrophy ($\langle\omega^2\rangle$ for Leray-α and in the DNS, $\langle\boldsymbol{\omega}\cdot\bar{\boldsymbol{\omega}}\rangle$ for LANS-α and Clark-α). DNS (Re$\approx$3300) is shown as solid black lines, LANS-α as dotted red, Clark-α as dashed green, and Leray-α as blue dash-dotted. An under-resolved (384^3) Navier–Stokes run is shown as a pink dash-triple-dotted line.

Kármán–Howarth scaling for scales smaller than α for both LANS-α and Clark-α. In particular, we note the observed scaling for Clark-α verifies the $vu^2 \sim l$ scaling and not the (theoretically possible) $vu^2 \sim l^{-1}$ $(u^3 \sim l)$ scaling. The predicted scaling is not observed in Leray due to its reduced effective Reynolds number. With these scalings in hand, we may proceed to observe the scaling of the longitudinal structure functions,

$$S_p^v(l) \equiv \langle (\delta v_\parallel^2)^{p/2} \rangle, \tag{66}$$

where we again replace the H_α^1 norm, i.e., $\langle |\delta v_\parallel||\delta u_\parallel| \rangle$, for the L^2 norm, i.e., $\langle (\delta v_\parallel)^2 \rangle$, in the case of Clark-$\alpha$ and LANS-α. We utilize the extended self-similarity hypothesis,[48–50] which proposes the scaling

$$S_p^v(l) \propto \left[L^{(\alpha,L)}(l)\right]^{\xi_p},$$

and normalize the results by ξ_3 to better visualize the deviation from linearity (which serves as a measure of intermittency). As we will show in the next section, our flow is anisotropic in the z direction. Therefore, structure functions are computed in horizontal planes only. The results are displayed in Fig. 4.

In Fig. 4, we may observe the intermittency properties of the models at subfilter scales. We note a reduced intermittency for both Leray-α and the Re$\approx$1300 DNS. This is consistent with the smoother, more laminar fields (due to the reduction of the effective Re) possessed by both. Interestingly, though LANS-α and Clark-α both possess the same cascade scaling [Eq. (23), as confirmed in Fig. 3], the Clark-α model is markedly more intermittent than LANS-α. If artificially truncated local interactions (in spectral space) is taken as a cause of enhanced intermittency,[51,52] then the increased intermittency observed in Clark-α is the expected result of truncation of the higher-order terms in the subfilter-stress tensor. Moreover, if the LANS-α's $\sim k^1$ spectrum is indeed associated with rigid bodies, these would serve to decrease the intermittency (no internal degrees of freedom being available in a rigid body), which is consistent with the results shown here. Due to this effect, LANS-α of the three regularization models most resembles the high-order intermittency of Navier–Stokes at subfilter scales.

IV. SGS POTENTIAL OF THE REGULARIZATIONS

A. Reproduction of superfilter-scale properties

The differences at subfilter scales between the regularizations and Navier–Stokes are important to understand how the models may be improved upon. From a practical standpoint, an equally important question is how they predict the superfilter-scale properties of a DNS when employed as models. This gives an indication of their SGS modeling potential. For this, we choose $\alpha = 2\pi/40$ corresponding to an optimal α-LES.[34] Note that the value of α has been optimized for neither Clark-α nor Leray-α; as a consequence, these models might perform better in other parameter regimes than the results indicate in this study.

Figure 5 gives the time evolution of the enstrophy of the DNS and the models along with that of an under-resolved Navier–Stokes solution at a resolution of 384^3 [$\nu = 3\times10^{-4}$, (pink online) dash-triple-dotted line]. We see that both LANS-α and Clark-α reproduce the proper amount of dissipation and are within 10% of the time required by the DNS to reach a statistical turbulent steady state. As has been observed before, Leray-α is under-dissipative.[15] We also note that it takes longer than the other models to reach a steady state even with the smaller filter width ($2\pi/40$, as opposed to $2\pi/13$). When compared to the larger α case, we see that the dissipation is much greater and the time scale to reach a turbulent steady state is decreased for Leray-α.

Compensated spectra averaged over several eddy turnover times are shown for the SGS case (i.e., k_α=40) in Fig. 6. Note that as the subgrid models are averaged over a different time interval, no meaningful comparison to the DNS is possible for $k < k_F = 3$. Even without an optimal choice for the value of α, Clark-α best reproduces the DNS spectrum for scales larger than α. We compute root-mean-square spectral errors as recently introduced in Ref. 35,

Downloaded 17 Jun 2008 to 157.92.44.71. Redistribution subject to AIP license or copyright; see http://pof.aip.org/pof/copyright.jsp

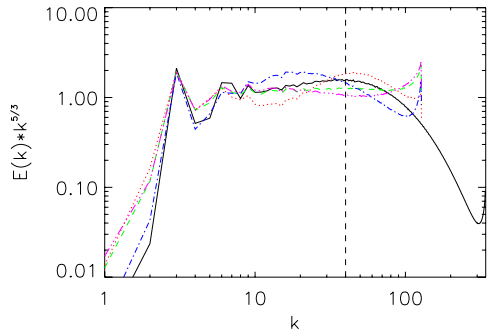

FIG. 6. (Color online) Spectra compensated by K41 for 1024^3 DNS ($\mathrm{Re}\approx 3300$) averaged over $t=[8.25,9]$. Labels are as in Fig. 5. The wavenumber corresponding to the filter width k_α is shown as a vertical dashed line. 384^3 simulations are averaged over $t\in[15,20]$. Note that to make a comparison for most wavenumbers, the spectra must be averaged within a turbulent steady state. Therefore, as the subgrid models are averaged over a different time interval, there is no meaningful comparison to the DNS for $k<3$. For LANS-α, we observe a contamination of the superfilter-scale spectrum (at $k\in[9,30]$) related to the steep subfilter-scale spectrum and the conservation of energy. Even though a different α (optimized with respect to spectral energy prediction at this numerical resolution) may provide better results for Clark-α, this model does very well at reproducing the large-scale energy spectrum. Leray-α's performance is the poorest.

$$\epsilon_p^b = \left[\frac{\Sigma_{k=k_F}^{k_\alpha} k^{2p}[E_{\mathrm{model}}(k)-E(k)]^2}{\Sigma_{k=k_F}^{k_\alpha} k^{2p}E^2(k)}\right]^{1/2}, \tag{67}$$

where k_F is the wavenumber for the forcing scale, $E(k)$ is the DNS spectrum [in the $L^2(v)$ norm], and $E_{\mathrm{model}}(k)$ is the subgrid model spectrum (in the appropriate norm). Another measure introduced in Ref. 35 is given by

$$\epsilon_p^a = \left[\frac{\left[\Sigma_{k=k_F}^{k_\alpha} k^{p}[E_{\mathrm{model}}(k)-E(k)]\right]^2}{\left(\Sigma_{k=k_F}^{k_\alpha} k^{p}E(k)\right)^2}\right]^{1/2}. \tag{68}$$

With $p=0$, we find the error in the total energy; i.e., $\epsilon_0^a \equiv \epsilon_E$. As this is dynamically controlled in our experiment, we find zero in all cases. For $p=2$, we find the error in the total dissipation, i.e., $\epsilon_2^a \equiv \epsilon_\varepsilon$, which is observed in Fig. 5. Every deviation from the DNS spectrum is counted positive, however, in ϵ_p^b. For $p=0$, we find the error in the energy spectrum: In decreasing order, $\epsilon_0^b=0.24$ for Leray-α, 0.23 for the under-resolved 384^3, 0.20 for LANS-α, and 0.16 for Clark-α. Both LANS-α and Clark-α improve the estimate over the under-resolved run, but Clark-α makes the best prediction. We see that only Clark-α improves the estimate of the power spectrum at this resolution for each scale considered separately (see Fig. 6). Leray-α performs the poorest of the three regularization models, but it is also not optimized. As previously argued, its effective Reynolds number is too low to accurately model the DNS flow. Either a decrease in the viscosity ν, or a decrease in the filter size α (and, hence, an increase in the nonlinearity), or both would likely improve the accuracy of Leray-α as an SGS model. Due to its frozen-in (or enslaved) rigid-body regions and its conservation of total energy, the LANS-α model cannot reproduce the DNS spectrum at superfilter scales unless α is only a few times larger than the dissipation scale.[34]

Another measure of the success of a subgrid model is the reproduction of structures in the flow. In Fig. 7 we have 3D volume rendering of the enstrophy density ω^2 ($\boldsymbol{\omega}\cdot\bar{\boldsymbol{\omega}}$ for LANS-α and Clark-α) for the DNS, the three SGS-model simulations ($k_\alpha=40$), the 384^3 under-resolved Navier–Stokes solution, all at a Reynolds number of ≈ 3300, and the $\mathrm{Re}\approx 1300$ DNS. Due to the late times depicted (longer than a Lyapunov time) there can be no point-by-point comparison between the simulations. Instead, we note that there are four horizontal bands where the forcing causes a maximum shear. This large-scale feature of the flow is missing only from Leray-α and the $\mathrm{Re}\approx 1300$ run. The three other runs reproduce this feature well (note that the apparently thicker tubes present in Clark-α are vortex tube mergers). The results lead again to the conclusion that the under-resolved Navier–Stokes, the Clark-α, and the LANS-α models are better subgrid models than Leray-α due to its reduced effective Re.

For the SGS models, the predicted l^1 from the de Kármán–Howarth theorem for Navier–Stokes is well reproduced by all models at superfilter scales (not depicted here). We may then proceed in Fig. 8 to analyze the SGS model intermittency results. We see that all models reproduce the intermittency up to the tenth-order moment within the error bars (although there is a small decrease in intermittency for Leray-α). Thus, we conclude that with adequately chosen values of α (and of ν for Leray-α), all three models can reproduce the intermittency of the DNS (to within the error bars).

The subfilter-scale physics of Leray-α shows that it possesses the smoothest solutions of the three models and reduces the effective Re. We have seen that this strongly hampers its effectiveness as a SGS model. "Rigid bodies" are observed in the subfilter scales of LANS-α (Ref. 34) that strongly influence even the superfilter-scale energy spectrum but not the subfilter-scale dissipation nor intermittency properties. These affects also carry over to its application as a SGS model in that very small filter widths are required to properly predict the large-scale spectrum. Clark-α's approximately k^{-1} subfilter energy spectrum is the closest to $k^{-5/3}$ of the three models and is seen to cause the least contamination of the superfilter-scale spectrum when employed as a SGS model. Finally, when the filter width is small enough, the enhanced intermittency of Clark-α is nearly eliminated.

B. Computational gains

The rationale behind using a SGS model is that it leads to adequate solutions at a reduced computational cost, because it computes fewer dof; indeed, for an SGS model, the ratio of Navier–Stokes's dof to the model's dof, a prediction for memory savings and hence computation time savings for

Downloaded 17 Jun 2008 to 157.92.44.71. Redistribution subject to AIP license or copyright; see http://pof.aip.org/pof/copyright.jsp

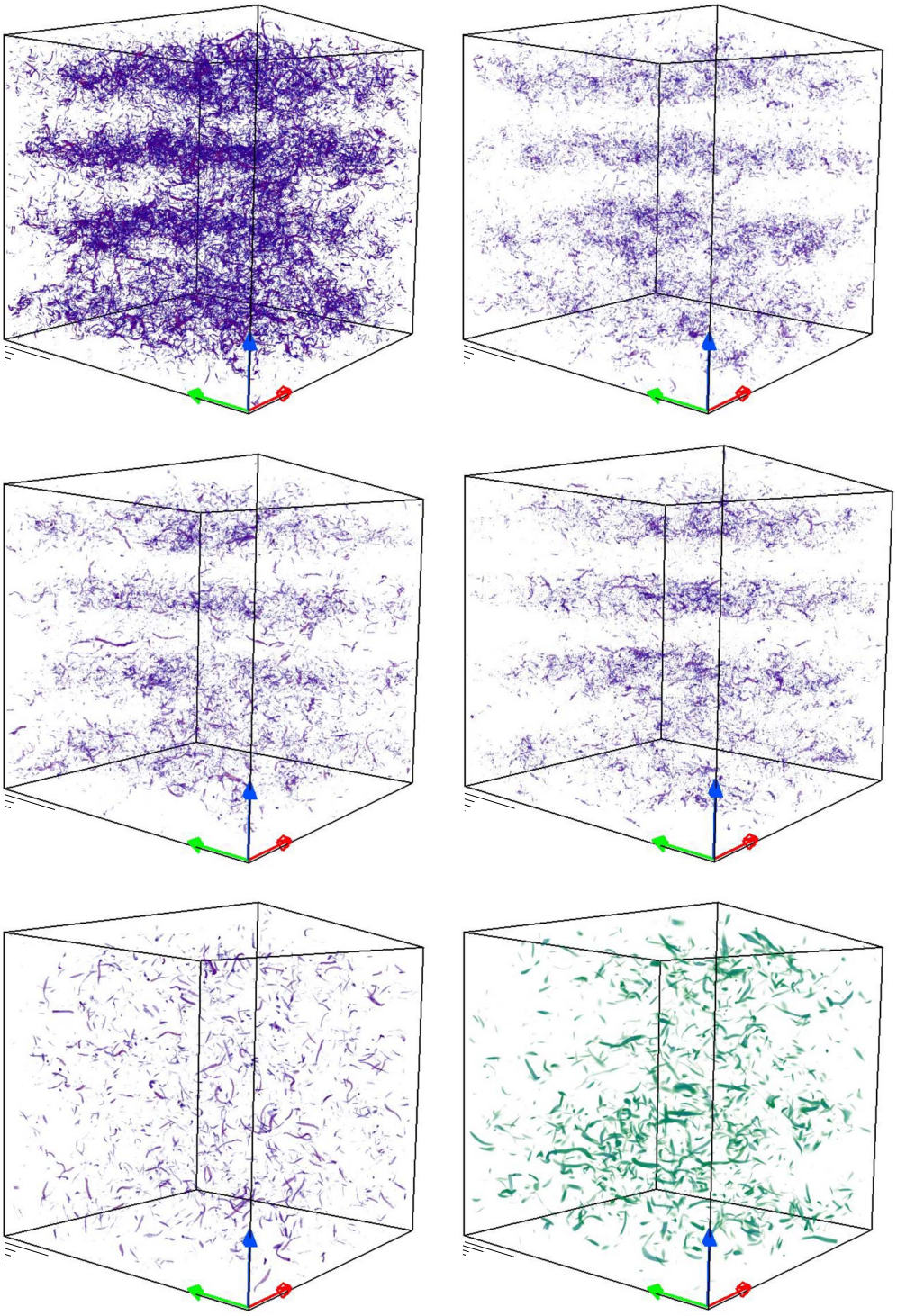

FIG. 7. (Color online) Volume rendering of the enstrophy density ω^2 ($\boldsymbol{\omega}\cdot\bar{\boldsymbol{\omega}}$ for LANS-α and Clark-α). The four lengths depicted are integral length scale $\mathfrak{L}$, Taylor scale λ, filter width α, and dissipative scale η_K as calculated separately for each simulation. First row, first column: $\mathrm{Re}\approx 3300$ DNS. Second row, first column: Clark-α. First row, second column: LANS-α. Second row, second column: Under-resolved Navier–Stokes. For the first two rows, the snapshot is for $t=9$. Third row, first column: Leray-α for $t=16$. Third row, second column: $\mathrm{Re}\approx 1300$ DNS for $t=19$, corresponding to their slower development of turbulence. For Leray-α, the locations of vortex tubes are consistent with a lower Re flow, while the other models (including under-resolving) reproduce the large-scale pattern of the flow well. The color scale indicates the strength of the enstrophy density, with dark grey shades (purple online) stronger than light grey shades (green online).

numerical simulation, is a crucial factor. Consequently, analytical bounds on the sizes of the attractors for the three regularization subgrid models may be useful indicators of their computational savings. The dof for LANS-α is derived in Ref. 29 and confirmed in Ref. 34,

$$\mathrm{dof}_\alpha \propto \frac{L}{\alpha}\mathrm{Re}^{3/2}, \tag{69}$$

where L is the integral scale (or domain size). We may compare this to the dof for Navier–Stokes,

Downloaded 17 Jun 2008 to 157.92.44.71. Redistribution subject to AIP license or copyright; see http://pof.aip.org/pof/copyright.jsp

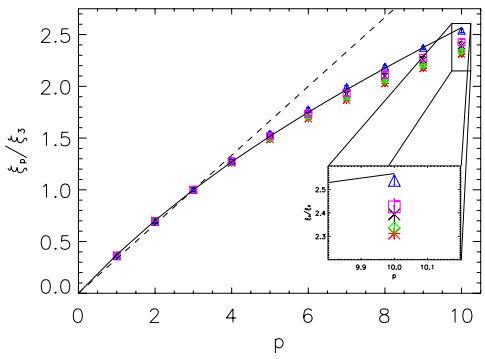

FIG. 8. (Color online) Normalized structure function scaling exponent ξ_p/ξ_3 vs order p. The dashed line indicates K41 scaling and the solid line the She-Lévêque formula (Ref. 53). The DNS results are indicated by black × marks. LANS-α by red asterisks, Clark-α by green diamonds, Leray-α by blue triangles, and pink boxes for the under-resolved Navier–Stokes run. With a small enough filter-width α, the intermittency properties of the DNS can be reproduced with all three models.

$$\mathrm{dof}_{\mathrm{NS}} \sim \left(\frac{L}{\eta_{\mathrm{K}}}\right)^3 \sim \mathrm{Re}^{9/4}, \tag{70}$$

which immediately yields

$$\frac{\mathrm{dof}_{\mathrm{NS}}}{\mathrm{dof}_{\alpha}} \sim \left(\frac{\alpha}{L}\right)\mathrm{Re}^{3/4}. \tag{71}$$

It was found, however, that to reproduce the superfilter-scale energy spectrum of an equivalent DNS, the filter width α must be no larger than a few times the dissipation scale η_{K}.[34] This is the result of the "polymerization" of the flow in LANS-α, and the associated $E(k) \sim k^1$ scaling at subfilter scales and consequent contamination at superfilter scales via energy conservation. With this added caveat, it follows that the reduction in dof is independent of Re (and a net factor of about 10). Our study here illustrates that the high-order structure functions may be reproduced for much larger values of α. Therefore, in applications where the spectrum is not of great concern, much greater reduction in numerical resolution would be feasible.

For Clark-α there is an upper bound on the Hausdorff (d_{H}) and fractal (d_F) dimensions of the attractor,

$$d_{\mathrm{H}} \leqslant d_F \leqslant C\left(\frac{L}{\eta_{\mathrm{K}}^C}\right)^3\left(\frac{L}{\alpha}\right)^{3/4}, \tag{72}$$

where η_{K}^C is the Kolmogorov dissipation length scale corresponding to the Clark-α model.[21] From its observed k^{-1} spectrum, we may estimate η_{K}^C or, equivalently, $k_\eta^C \sim 1/\eta_{\mathrm{K}}^C$. For dissipation the large wavenumbers dominate and, therefore, combining the Clark-α energy balance Eq. (6) with its subfilter scale energy spectrum Eq. (24) allows us to implicitly specify its dissipation wavenumber k_η^C by

$$\begin{aligned}\frac{\varepsilon_\alpha^C}{\nu} &\sim \int^{k_\eta^C} k^2 E_\alpha^C(k)dk \\ &\sim \int^{k_\eta^C} k^2(\varepsilon_\alpha^C)^{2/3}\alpha^{2/3}k^{-1}dk \\ &\sim (\varepsilon_\alpha^C)^{2/3}\alpha^{2/3}(k_\eta^C)^2.\end{aligned} \tag{73}$$

We then have

$$k_\eta^C \sim \frac{(\varepsilon_\alpha^C)^{1/6}}{\nu^{1/2}\alpha^{1/3}}. \tag{74}$$

It follows that

$$\frac{\mathrm{dof}_{\mathrm{NS}}}{\mathrm{dof}_{\mathrm{Clark}}} \sim \mathrm{Re}^{3/4}\left(\frac{\alpha}{L}\right)^{3/4}\alpha^{-1}. \tag{75}$$

This is similar to the prediction for LANS-α, but as energy spectra are more easily reproduced for larger values of α than with LANS-α (but not the intermittency properties), it may be the case that α is not tied to the Kolmogorov dissipation scale η_{K}. If so, then the computational saving might increase as $\mathrm{Re}^{3/4}$, which is promising for use of Clark-α as an LES model. This conclusion is bolstered to the extent that the results in Sec. IV A for k_α=40 ($\alpha \approx 7\eta_{\mathrm{K}}$) are acceptable. If even further separation from the dissipative scale is not possible, there is still a greater reduction in dof (a factor of 20) for Clark-α than for LANS-α.

For Leray-α, we have the following upper bounds on the Hausdorff dimension (d_{H}) and fractal dimension (d_F) of the global attractor,

$$d_{\mathrm{H}} \leqslant d_F \leqslant c\left(\frac{L}{\eta_{\mathrm{K}}^{\mathrm{L}}}\right)^{12/7}\left(1+\frac{L}{\alpha}\right)^{9/14}, \tag{76}$$

where $\eta_{\mathrm{K}}^{\mathrm{L}}$ is the dissipation length scale for Leray-α.[14] Again, we estimate the dissipation wavenumber for Leray-α $k_\eta^{\mathrm{L}} \sim 1/\eta_{\mathrm{K}}^{\mathrm{L}}$. From Eqs. (38) and (49), that is, assuming the $k^{-1/3}$ spectrum resulting from the de Kármán–Howarth equation, we find

$$\begin{aligned}\frac{\varepsilon^{\mathrm{L}}}{\nu_{\mathrm{L}}} &\sim \int^{k_\eta^{\mathrm{L}}} k^2 E^{\mathrm{L}}(k)dk \\ &\sim \int^{k_\eta^{\mathrm{L}}} k^2(\varepsilon^{\mathrm{L}})^{2/3}\alpha^{4/3}k^{-1/3}dk \\ &\sim (\varepsilon^{\mathrm{L}})^{2/3}\alpha^{4/3}(k_\eta^{\mathrm{L}})^{8/3}.\end{aligned} \tag{77}$$

Consequently we have

$$k_\eta^{\mathrm{L}} \sim \frac{(\varepsilon^{\mathrm{L}})^{1/8}}{\nu_{\mathrm{L}}^{3/8}\alpha^{1/2}}. \tag{78}$$

It follows that

$$\frac{\mathrm{dof}_{\mathrm{NS}}}{\mathrm{dof}_{\mathrm{Leray}}} \sim \frac{L^{9/7}\nu^{-9/4}}{\nu_{\mathrm{L}}^{-9/14}\alpha^{-6/7}\left(1+\frac{L}{\alpha}\right)^{9/14}}. \tag{79}$$

Our results suggest that for an effective LES the viscosity ν_{L} must be chosen to be *smaller* than ν. This leads to an upper bound on the computational savings for Leray-α,

Downloaded 17 Jun 2008 to 157.92.44.71. Redistribution subject to AIP license or copyright; see http://pof.aip.org/pof/copyright.jsp

$$\frac{\mathrm{dof}_{\mathrm{NS}}}{\mathrm{dof}_{\mathrm{Leray}}} < C\frac{\mathrm{Re}^{45/28}\alpha^{6/7}}{\left(1+\frac{L}{\alpha}\right)^{9/14}}. \tag{80}$$

If we further assume that α is directly proportional to the dissipative scale η_{K}, we arrive at

$$\frac{\mathrm{dof}_{\mathrm{NS}}}{\mathrm{dof}_{\mathrm{Leray}}} < C\mathrm{Re}^{27/56}, \tag{81}$$

which is not exceedingly promising for use as a LES. All such estimates are, however, purely conjectural until the proper choices of α and ν_L are determined.

V. DISCUSSION

We derived the de Kármán–Howarth equations for the Leray-α and Clark-α models. These two models may be viewed as successive truncations of the subfilter-scale stress of the Lagrangian-averaged Navier–Stokes α-model (LANS-α). In the case of Clark-α two different inertial range scalings follow from the dimensional analysis of this equation. The case of Leray-α is simpler as a single scaling is predicted. This is the case for Navier–Stokes and LANS-α as well. To our knowledge, we computed the first numerical solution of the Clark-α model, the results of which are encouraging for further study. We compared these to solutions for a 1024^3 DNS under periodic boundary conditions ($\nu=3\times10^{-4}$, $\mathrm{Re}\approx3300$) using a 384^3 resolution under the same exact conditions for LANS-α, Leray-α, Clark-α, and an under-resolved 384^3 solution of the Navier–Stokes equations. We employed two different filter widths α. The first choice $\alpha=2\pi/13$ was used to understand the subfilter-scale physics and the second choice $\alpha=2\pi/40$ was employed to test the SGS potential of the models. In comparing these two choices, we found for Leray-α that an increase in α substantially decreases the nonlinearity (and hence decreases the effective Reynolds number Re). For this reason, we were unable to confirm either the inertial range scaling from its de Kármán–Howarth equation or its subfilter-scale energy spectrum. For Clark-α, we were able to determine the dominant de Kármán–Howarth inertial range scaling to be $u^2v\sim l$, which leads to the associated k^{-1} energy spectrum, also indicated by our results.

The performance of the three regularizations as SGS models (for a resolution of 384^3 and $k_\alpha=40$) was comparable to that of the under-resolved Navier–Stokes solution in reproducing the DNS energy spectrum at superfilter scales. Only Clark-α showed a clear improvement in approximating the spectrum. From 3D volume rendering of enstrophy density, we found that Clark-α and LANS-α were comparable to the under-resolved solution. Even at $\alpha=2\pi/40$, Leray-α's 3D spatial structures are consistent with a significantly reduced Re flow (e.g., comparable to a $\mathrm{Re}\approx1300$ DNS). We note that the value of α was chosen optimally for LANS-α at the resolution of 384^3, and that for Clark-α (and especially for Leray-α) smaller resolutions (greater computational savings) may have comparable results for this value of α. Such a comparison is beyond the scope of the present work.

Although LANS-α and Clark-α exhibit the same inertial range scaling arising from similarities in their de Kármán–Howarth equations, Clark-α is decidedly more intermittent than Navier–Stokes at subfilter scales. At the same time, LANS-α is only slightly more intermittent than Navier–Stokes. These results are consistent with the artificial truncation of local nonlinear interactions (in spectral space) in the SGS stress tensor of each model. This effect is reduced for LANS-α by the "rigid-body regions" enslaved in its larger scale flow which possess no internal degrees of freedom. The reduced intermittency observed for Leray-α is related to its smoother, more laminar fields as a result of its reduced effective Re.

Finally, we analyzed the reduction in the number of dof in the models, as compared to Navier–Stokes (and, hence, their LES potential based on their computational savings). We noted that as LANS-α reproduces the intermittency properties of a DNS quite well even for larger values of α, some further reduction in numerical saving might be achieved provided the contamination due to its k^1 rigid-body energy spectrum were not important in a given application. As Clark-α possesses a similar reduction in dof to LANS-α, its LES potential is tied to the optimal value of α for LES. Our study indicates that Clark-α may be applicable (especially with regards to the energy spectrum) for larger values of α than LANS-α. In fact, if its optimal value is not a function of Re, the computational resolution savings increases as $\mathrm{Re}^{3/4}$ for Clark-α. For the case of Leray-α, the prediction is complicated by the effective reduction in Re as α increases. Prediction of optimized values of α and of effective dissipation ν_L are required to assess its LES potential. Future work should include such a study for both Leray-α and Clark-α.

All three regularizations were shown to be successful, in that their control of the flow gradient reduces the degrees of freedom and saves computation while preserving a properly defined Reynolds number (albeit for Leray-α that definition is not yet demonstrated). Clark-α accurately reproduces the total dissipation, the time scale to obtain a turbulent statistical steady state, and the large-scale energy spectrum of a DNS. These results seem to result from Clark-α being an order α^2 approximation of Navier–Stokes. We have shown that Leray-α reduces the effective Reynolds number of the flow. The last of the three models, LANS-α restores Kelvin's circulation theorem (advected by a smoothed velocity) and the conservation of a form of helicity. Using spectra as a measure of the success of a subgrid model, LANS-α is less than optimal, due to its contamination of the superfilter-scale spectrum. However, other measures of the success of a subgrid model are possible: For example, in regard to intermittency, LANS-α may be considered a superior model. For Clark-α, intermittency may be a function of filter width while for LANS-α, intermittency does not vary much with α.

Through examination of these three systems of nonlinear partial differential equations in comparison to Navier–Stokes, we have demonstrated that intermittency can be preserved with careful modification of the nonlinearity. This was seen with the LANS-α model and may be related to the conservation of small-scale circulation. Besides intermittency, the nonlinear terms also play a role in the energy spec-

Downloaded 17 Jun 2008 to 157.92.44.71. Redistribution subject to AIP license or copyright; see http://pof.aip.org/pof/copyright.jsp

trum (at both subfilter and superfilter scales) and in the dissipation. These terms must model both the nonlocal interactions (to recover the intermittency) but also the local interactions (which are too strongly suppressed inside the rigid bodies of LANS-α). Finally, we have demonstrated that regularization modeling can be employed to reduce the computational cost while preserving the high-order statistics of the flow.

We remark that the computational gain thus far achieved by any of these regularizations is insufficient for applications at very high Reynolds numbers, and the three subgrid stress tensors discussed here may need to be supplemented with an enhanced effective viscosity to be employed as LES. This is a common practice when implementing the Clark model (see, e.g., Ref. 19 for a study of this model with an extra Smagorinsky term). In this light, the present study may be useful as an analysis of the properties of the SGS tensors of the regularizations, and to pick best candidates, before the addition of enhanced dissipation. Studies similar to that in Ref. 34 will also need to be done for the cases of Clark-α and Leray-α to quantify their computational savings before the addition of such dissipative terms.

ACKNOWLEDGMENTS

The National Center for Atmospheric Research is sponsored by the National Science Foundation. Computer time provided at NCAR is gratefully acknowledged, as well as NSF-CMG Grant No. 0327888. The work of D.D.H. was partially supported by the U.S. Department of Energy, Office of Science, Advanced Scientific Computing Research, and by the Royal Society of London Wolfson Award for Meritorious Research.

[1] U. Frisch, *Turbulence: The Legacy of A. N. Kolmogorov* (Cambridge University Press, Cambridge, 1995).
[2] A. N. Kolmogorov, "The local structure of turbulence in incompressible viscous fluid for very large Reynolds numbers," Dokl. Akad. Nauk SSSR **30**, 299 (1941); Reprinted in Proc. R. Soc. London, Ser. A **434**, 9 (1991).
[3] A. N. Kolmogorov, "On degeneration (decay) of isotropic turbulence in an incompressible viscous liquid," Dokl. Akad. Nauk SSSR **31** 538 (1941).
[4] A. N. Kolmogorov, "Dissipation of energy in locally isotropic turbulence," Dokl. Akad. Nauk SSSR **32**, 16 (1941); Reprinted in Proc. R. Soc. London, Ser. A **434**, 15 (1991).
[5] C. Meneveau and J. Katz, "Scale-invariance and turbulence models for large-eddy simulation," Annu. Rev. Fluid Mech. **32**, 1 (2000).
[6] Y. Kaneda, T. Ishihara, M. Yokokawa, K. Itakura, and A. Uno, "Energy dissipation rate and energy spectrum in high resolution direct numerical simulations of turbulence in a periodic box," Phys. Fluids **15**, L21 (2003).
[7] Y. Tsuji, "Intermittency effect on energy spectrum in high-Reynolds number turbulence," Phys. Fluids **16**, L43 (2004).
[8] A. Alexakis, P. D. Mininni, and A. Pouquet, "Imprint of large-scale flows on turbulence," Phys. Rev. Lett. **95**, 264503 (2005).
[9] P. D. Mininni, A. G. Pouquet, and D. C. Montgomery, "Small-scale structures in three-dimensional magnetohydrodynamic turbulence," Phys. Rev. Lett. **97**, 244503 (2006).
[10] S. Chen, D. D. Holm, L. G. Margolin, and R. Zhang, "Direct numerical simulations of the Navier–Stokes alpha model," Physica D **133**, 66 (1999).
[11] B. J. Geurts and D. D. Holm, "Leray simulation of turbulent shear layers," in *Advances in Turbulence IX: Proceedings of the Ninth European Turbulence Conference*, edited by J. P. Castro and P. E. Hancock (CIMNE, Barcelona, 2002), pp. 337.
[12] B. J. Geurts and D. D. Holm, "Regularization modeling for large-eddy simulation," Phys. Fluids **15**, L13 (2003).
[13] D. D. Holm and B. Nadiga, "Modeling mesoscale turbulence in the barotropic double gyre circulation," J. Phys. Oceanogr. **33**, 2355 (2003).
[14] A. Cheskidov, D. D. Holm, E. Olson, and E. S. Titi, "On a Leray-α model of turbulence," Proc. R. Soc. London, Ser. A **461**, 629 (2005).
[15] B. J. Geurts and D. D. Holm, "Leray and LANS-α modelling of turbulent mixing," J. Turbul. **7**, 1 (2006).
[16] J. Leray, "Essai sur le mouvement d'un fluide visqueux emplissant l'espace," Acta Math. **63**, 193 (1934).
[17] A. Leonard, "Energy cascade in large-eddy simulations of turbulent fluid flows," in *Turbulent Diffusion in Environmental Pollution; Proceedings of the Second Symposium*, Charlottesville, VA, 8–14 April 1973 (Academic, New York, 1974), Volume A, A75-30951 13-47, pp. 237–248.
[18] R. A. Clark, J. H. Ferziger, and W. C. Reynolds, "Evaluation of subgrid-scale models using an accurately simulated turbulent flow," J. Fluid Mech. **91**, 1 (1979).
[19] G. S. Winckelmans, A. A. Wray, O. V. Vasilyev, and H. Jeanmart, "Explicit-filtering large-eddy simulation using the tensor-diffusivity model supplemented by a dynamic Smagorinsky term," Phys. Fluids **13**, 1385 (2001).
[20] D. Carati, G. S. Winckelmans, and H. Jeanmart, "On the modelling of the subgrid-scale and filtered-scale stress tensors in large-eddy simulation," J. Fluid Mech. **441**, 119 (2001).
[21] C. Cao, D. D. Holm, and E. S. Titi, "On the Clark α model of turbulence: Global regularity and long-time dynamics," J. Turbul. **6**, 19 (2005).
[22] D. D. Holm, J. E. Marsden, and T. S. Ratiu, "The Euler–Poincaré equations and semidirect products with applications to continuum theories," Adv. Math. **137**, 1 (1998).
[23] S. Chen, C. Foias, D. D. Holm, E. Olson, E. S. Titi, and S. Wynne, "Camassa–Holm equations as a closure model for turbulent channel and pipe flow," Phys. Rev. Lett. **81**, 5338 (1998).
[24] S. Chen, C. Foias, D. D. Holm, E. Olson, E. S. Titi, and S. Wynne, "The Camassa–Holm equations and turbulence," Physica D **133**, 49 (1999).
[25] S. Chen, C. Foias, D. D. Holm, E. Olson, E. S. Titi, and S. Wynne, "A connection between the Camassa–Holm equations and turbulent flows in channels and pipes," Phys. Fluids **11**, 2343 (1999).
[26] D. D. Holm, J. E. Marsden, and T. S. Ratiu, "Euler–Poincaré models of ideal fluids with nonlinear dispersion," Phys. Rev. Lett. **80**, 4173 (1998).
[27] D. D. Holm, "Lagrangian averages, averaged Lagrangians, and the mean effects of fluctuations in fluid dynamics," Chaos **12**, 518 (2002).
[28] D. D. Holm, "Averaged Lagrangians and the mean effects of fluctuations in ideal fluid dynamics," Physica D **170**, 253 (2002).
[29] C. Foias, D. D. Holm, and E. S. Titi, "The Navier–Stokes-alpha model of fluid turbulence," Physica D **152-153**, 505 (2001).
[30] D. C. Montgomery and A. Pouquet, "An alternative interpretation for the Holm 'alpha model'," Phys. Fluids **14**, 3365 (2002).
[31] H. Zhao and K. Mohseni, "A dynamic model for the Lagrangian-averaged Navier–Stokes-α equations," Phys. Fluids **17**, 5106 (2005).
[32] K. Mohseni, B. Kosović, S. Shkoller, and J. E. Marsden, "Numerical simulations of the Lagrangian averaged Navier–Stokes equations for homogeneous isotropic turbulence," Phys. Fluids **15**, 524 (2003).
[33] B. J. Geurts and D. D. Holm "Alpha-modeling strategy for LES of turbulent mixing," in *Turbulent Flow Computation*, edited by D. Drikakis and B. J. Geurts (Kluwer Academic, London, 2002), pp. 237.
[34] J. Pietarila Graham, D. Holm, P. Mininni, and A. Pouquet, "Highly turbulent solutions of the Lagrangian-averaged Navier–Stokes alpha model and their large-eddy-simulation potential," Phys. Rev. E **76**, 056310 (2007).
[35] J. Meyers, P. Sagaut, and B. J. Geurts, "Optimal model parameters for multi-objective large-eddy simulations," Phys. Fluids **18**, 5103 (2006).
[36] T. de Kármán and Leslie Howarth, "On the statistical theory of isotropic turbulence," Proc. R. Soc. London, Ser. A **164**, 192 (1938).
[37] D. D. Holm, "Kármán Howarth theorem for the Lagrangian-averaged Navier Stokes alpha model of turbulence," J. Fluid Mech. **467**, 205 (2002).
[38] R. H. Kraichnan, "Inertial ranges in two-dimensional turbulence," Phys. Fluids **10**, 1417 (1967).
[39] M. van Reeuwijk, H. J. J. Jonker, and K. Hanjalić, "Incompressibility of the Leray-α model for wall-bounded flows," Phys. Fluids **18**, 018103 (2006).
[40] D. O. Gómez, P. D. Mininni, and P. Dmitruk, "Parallel simulations in turbulent MHD," Phys. Scr., T **116**, 123 (2005).
[41] D. O. Gómez, P. D. Mininni, and P. Dmitruk, "MHD simulations and astrophysical applications," Adv. Space Res. **35**, 899 (2005).
[42] G. I. Taylor and A. E. Green, "Mechanism of the production of small eddies from large ones," Proc. R. Soc. London, Ser. A **158**, 499 (1937).
[43] P. D. Mininni, Y. Ponty, D. C. Montgomery, J.-F. Pinton, H. Politano, and

Downloaded 17 Jun 2008 to 157.92.44.71. Redistribution subject to AIP license or copyright; see http://pof.aip.org/pof/copyright.jsp

A. Pouquet, "Dynamo regimes with a nonhelical forcing," Astrophys. J. **626**, 853 (2005).
[44]M. Brachet, "The geometry of small-scale structures in a Taylor–Green vortex," Academie des Sciences Paris Comptes Rendus Serie Sciences Mathematiques **311**, 775 (1990).
[45]Y. Ponty, P. D. Mininni, D. C. Montgomery, J.-F. Pinton, H. Politano, and A. Pouquet, "Numerical study of dynamo action at low magnetic Prandtl numbers," Phys. Rev. Lett. **94**, 164502 (2005).
[46]P. Sagaut, *Large Eddy Simulation for Incompressible Flows*, 3rd ed. (Springer, Berlin, 2006).
[47]P. D. Mininni, A. Alexakis, and A. Pouquet, "Large-scale flow effects, energy transfer, and self-similarity on turbulence," Phys. Rev. E **74**, 016303 (2006).
[48]R. Benzi, S. Ciliberto, C. Baudet, G. Ruiz Chavarria, and R. Tripiccione, "Extended self-similarity in the dissipation range of fully developed turbulence," Europhys. Lett. **24**, 275 (1993).
[49]R. Benzi, S. Ciliberto, R. Tripiccione, C. Baudet, F. Massaioli, and S. Succi, "Extended self-similarity in turbulent flows," Phys. Rev. E **48**, R29 (1993).
[50]R. Benzi, L. Biferale, S. Ciliberto, M. V. Struglia, and R. Tripiccione, "Scaling property of turbulent flows," Phys. Rev. E **53**, R3025 (1996).
[51]J.-P. Laval, B. Dubrulle, and S. Nazarenko, "Nonlocality and intermittency in three-dimensional turbulence," Phys. Fluids **13**, 1995 (2001).
[52]B. Dubrulle, J.-P. Laval, S. Nazarenko, and O. Zaboronski, "A model for rapid stochastic distortions of small-scale turbulence," J. Fluid Mech. **520**, 1 (2004).
[53]Z. She and E. Leveque, "Universal scaling laws in fully developed turbulence," Phys. Rev. Lett. **72**, 336 (1994).

Downloaded 17 Jun 2008 to 157.92.44.71. Redistribution subject to AIP license or copyright; see http://pof.aip.org/pof/copyright.jsp